

This paper was recommended for publication in revised form by Regional Editor Mohammed Sajjad Mayeed

FUNDAMENTAL ASSESSMENTS AND NEW ENABLING PROPOSALS FOR HEAT TRANSFER CORRELATIONS AND FLOW REGIME MAPS FOR SHEAR DRIVEN CONDENSERS IN THE ANNULAR/STRATIFIED REGIME

***A. Narain**

Michigan Technological University
 Houghton, Michigan, United States

R. R. Naik

Michigan Technological University
 Houghton, Michigan, United States

S. Ravikumar

Michigan Technological University
 Houghton, Michigan, United States

S. S. Bhasme

Michigan Technological University
 Houghton, Michigan, United States

Keywords: mm-scale condensers, annular condensation, heat-transfer rate correlations, flow regime transition

* Corresponding author: A. Narain, Phone: (906) 487-2555, Fax: (906) 487-2822

E-mail address: narain@mtu.edu

ABSTRACT

Modern-day applications need mm-scale shear-driven flow condensers. Condenser designs need to ensure large heat transfer rates for a variety of flow conditions. For this, good estimates for heat-transfer rate correlations and correlations for the length of the annular regime (beyond which plug-slug flows typically occur) are needed. For confident use of existing correlations (particularly the more recent ones supported by large data sets) for shear-pressure driven internal condensing flows, there is a great need to relate the existing correlation development approaches to direct flow-physics based fundamental results from theory, computations, and experiments. This paper addresses this need for millimeter scale shear driven and annular condensing flows. In doing so, the paper proposes/compares a few new and reliable non-dimensional heat-transfer coefficient correlations as well as a key flow regime transition criteria/correlation.

INTRODUCTION

There is a critical need for thermal management systems with reduced mass and size which are capable of handling ever-increasing high heat loads at small to moderate temperature differences and high heat-flux values ([1, 2]). This need is particularly evidenced in requirements of high-power consumption electronics industry. To achieve this, one needs to develop innovative condensers and boilers (see [3-5]) that operate in the annular regime and are shear driven with

negligible effects of gravity. By shear driven, it is meant that the liquid condensate is driven by interfacial shear whereas the overall flow is driven by inlet mass flow rate and device-level pressure-differences. This paper focuses on addressing base-design needs for operating millimeter scale shear driven condensers in a non-pulsatile steady mode. Advantages of operating these condensers in a pulsatile mode are discussed in [3, 4]. Such millimeter scale condensers (and boilers [3]) are also of great value in the design of next generation space-based thermal systems, and gravity insensitive aircraft-based systems (including avionics cooling).

Traditional macro-scale internal flow condensers operating in vertical or inclined orientations relative to Earth's gravitational vector give rise to what are known as gravity-driven flows. Macro-scale horizontal flow condensers often (unless the flow rate is sufficiently fast [6]) operate in gravity-assisted mode because azimuthal direction condensate motion is significantly gravity driven in the annular/stratified mode. Gravity-driven or gravity-assisted annular/stratified flows are generally more stable. Furthermore available empirical/computational results for gravity driven/assisted flow condensers are well known and reasonably reliable (see [6, 7]).

The absence of flow direction gravity component in the shear driven condensers causes problematic non-annular flow regimes – which are thermally and hydro-dynamically inefficient – to appear and cover a significant portion of the condenser length (particularly if complete condensation is a

design requirement). These inefficient non-annular flow regimes are commonly categorized as plug flow, slug flow, and bubbly flow ([8-13]). Since analogous flow regimes are observed in adiabatic gas-liquid flows inside a duct, flow-regime map results ([6, 8-11]), heat-transfer coefficient (HTC) correlation results ([12]), and pressure-drop results ([13]) for phase-change flows largely employ terminologies (such as quality X , the ratio of vapor or gas-phase mass flow rate to total mass flow rate) that are prevalent and natural to large diameter in-tube adiabatic air-water type gas-liquid flow studies ([8, 9]).

A look at internal steady condensing and boiling flows (see [3-7], and Figs. 1-3) quickly establishes the fact that quality X strongly depends on physical distance from the inlet and thermal boundary conditions (i.e. the method of cooling/heating for condensers/boilers). Though there exist procedures ([14]) to relate existing flow-regime maps ([6, 8-11]), heat-transfer coefficient (HTC) correlations ([12]), and pressure-drop results ([13]) for a phase-change flow to a device's downstream physical distance and thermal boundary conditions; the descriptions are indirect and masked by prevalence of adiabatic two-phase flow terminologies that raise doubt on the validity of the heat-transfer correlations or introduce opacity in the direct use of flow regime maps. Furthermore many flow regime maps are often not properly non-dimensional or suitably differentiated by flow-physics – making it difficult to use them for tube-diameters and/or fluids different than the ones used in the underlying experimental data (even if their repeatability and reliability is assumed).

For mm-scale shear driven condensers, this paper addresses the need for proper flow-physics based new HTC correlations, annular to non-annular flow regime transition maps, and the need to relate them to existing correlation and criteria (particularly the more recent ones supported by large data sets). The approach's relationship to direct flow-physics based fundamental results from theory, computations, and experiments are described.

The flow morphologies or liquid-vapor configurations play a critical role in the determination of heat and mass transfer rates associated with internal condensing flows. The goal of a high performance condenser is to lengthen its annular/stratified flow regime (e.g., through introduction and control of recirculating vapor flow rates as shown in [3]) and to operate entirely in this regime. Hence it is important to predict and avoid the conditions that are associated with transition from annular to non-annular regimes. Several flow regime maps are available in literature ([8-11], etc.) that can provide estimates with regard to which flow regime is likely to occur for different device operation conditions – but this is only possible if they are properly non-dimensionalized, categorized, and extended (also see [15, 16]) to make them applicable to different fluids, diameters, cooling conditions, etc. Specifically, with regard to the length x_A of the annular zone in Fig.3, fundamental stability-theory based estimates are obtained from direct numerical simulations ([16-18]) and are used here to supplement existing empirical knowledge ([12, 13]) to present more confident estimates (both for horizontal earth-based and zero-gravity shear driven annular condensing flows).

Once the conditions favorable for realizing annular/stratified flows are identified and implemented ([3]), estimates for the heat-transfer coefficient (HTC) and pressure-drops is required for designing and sizing condensers for the operating heat loads. There are several semi-empirical correlations available in the literature ([12, 19-21]) that present equations to calculate the heat-transfer coefficient. Most of these studies focus on providing HTC estimates for the annular/stratified regime since that is the primary flow regime of interest. A key objective of this paper is to provide a structure and approach for examining the validity of existing semi-empirical heat-transfer correlations and, also, for future development of such correlations (including other regimes of condensing flows as well as boiling flows). An assessment of the structure of what non-dimensional parameters (or equivalent sets of numbers) should affect these HTC correlations is provided. The results/correlations from the studies available in literature ([12, 19-21]) are compared with results/correlations that are obtained and proposed in this study. This is done by using a combination of experimental data ([3, 4]), an approximate 1-D condensing flow simulation tool ([7]), and a nearly exact scientific 2-D steady/unsteady simulation tool ([16-18]). The mathematical models and the two simulation tools used in aiding this development are described in separate papers ([22, 23]).

The effect of the presence of wave-structures on the proposed HTC correlations, the factors causing the wave-structures, and the methodology to obtain empirical correction factors to incorporate these effects are also discussed.

2. PHYSICS BASED UNDERSTANDING AND MODEL STRUCTURES FOR HEAT TRANSFER COEFFICIENTS AND FLOW REGIME MAPS

This study focuses primarily on shear-driven annular flow condensation on: the bottom wall of horizontal channels, any one of the walls of a channel in zero-gravity, or on the inner wall of a circular-tube with the flow being shear driven and annular (as in mm-scale, moderate to large mass-flux, and negligible gravity terrestrial cases or in zero-gravity). The definition of annular and other condensing flow regimes (plug/slug, dispersed, bubbly, etc.) are available in [7-9] etc. A representative annular or stratified internal condensing two-dimensional flow in a channel (which is approximately the same as bottom wall condensation in rectangular cross-section ducts of small height 'h' to width 'w' ratios) is shown in Fig.1. The condensation is on the bottom wall which is kept at a temperature $T_w(x)$ lower than the saturation temperature (i.e., allowing for flow direction variations in wall temperature, $T_w(x) = T_{sat}(p_{in}) - \Delta T(x)$ where $\Delta T(x) > 0$). Film-wise condensation is realized because the surface is assumed to be *wetting* and $\Delta T(x)$ is assumed to be sufficiently large at all x locations (say $> 2-3^\circ\text{C}$).

In Fig.1, there is no condensation on the upper plate because its temperature T_{wu} is kept above (say by 5°C) the saturation temperature $T_{sat}(p_{in})$. If all the conditions for the flow in Fig.1 are retained except that the upper-surface temperature T_{wu} is changed to be equal to the lower surface temperature, then

there will be condensation on the upper plate as well - and the condensate motion may also be influenced by the presence of transverse-gravity. For inlet vapor velocities U_{in} below a certain critical speed U_{cr1} , the presence of transverse-gravity does not allow film-wise condensation on the upper surface of the condenser and liquid will drip down (compare Fig. 1 and Fig. 2A with its channel height satisfying: $h_{II} = h$). Therefore, if flow in Fig. 1 corresponding to the flow in Fig. 2A is realized for $U_{in} < U_{cr1}$, the flow is said to be “stratified” as transverse gravity plays a role in stabilizing the condensate motion (just as it plays a role in destabilizing the upper condensate motion in Fig. 2A). However, for inlet vapor velocity U_{in} above a certain critical speed U_{cr2} with $U_{cr2} > U_{cr1}$, separated vapor-liquid flow (i.e. film condensation on both the upper and lower surfaces) is known to prevail for a substantial length of the condenser (see Fig. 2B). Therefore, if flow in Fig. 1 corresponding to the flow in Fig. 2A is realized for $U_{in} > U_{cr2}$, the flow is said to be “annular” or “wavy annular” as interfacial shear and not transverse gravity plays the more significant role in stabilizing the condensate motion. The inlet speed range $U_{cr1} < U_{in} < U_{cr2}$ is said to correspond to the “transition” zone and is sometimes marked as shown in the Baker map ([9]) for larger diameter tubes and discussed later on in this paper for mm-scale shear driven condensers. For purposes of this paper, we term the flow regime in Fig. 1 “annular/stratified” and the term means to include all the aforementioned regimes termed “stratified,” “annular,” and “transition.”

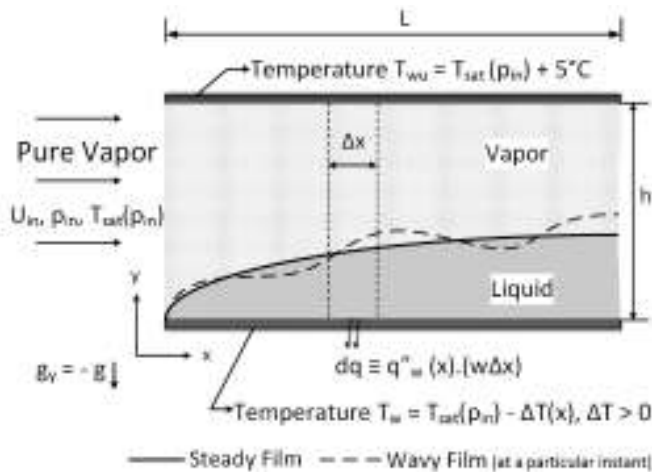


FIGURE 1: SCHEMATIC OF AN ANNULAR/STRATIFIED INTERNAL CONDENSING FLOW INSIDE A HORIZONTAL RECTANGULAR CROSS-SECTION CHANNEL.

For millimeter-scale condensers of primary interest, if the length L of the channel is sufficiently long (see Fig. 3), then the annular/stratified condensing flow regime typically transitions (see [12] and [3]) to plug/slug regimes at downstream distances $x > x_A$. As in Fig. 3, the end of the annular regime will be modeled by a sharp location $x \approx x_A$ with the understanding that, in reality, there is a transition zone between the annular and the plug/slug regimes.

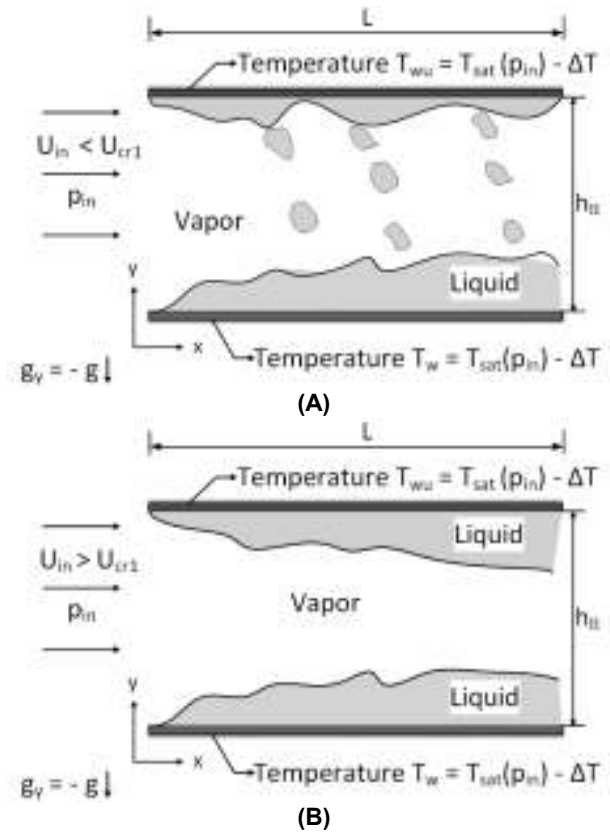


FIGURE 2: SCHEMATIC OF A SYMMETRICALLY COOLED HORIZONTAL CHANNEL WITH CONDENSATION ON BOTH UPPER AND LOWER SURFACES SHOWING:(A) FOR $U_{in} < U_{cr1}$, A SEPARATED ANNULAR/STRATIFIED FLOW IS NOT POSSIBLE; (B) FOR $U_{in} > U_{cr2}$, BUT LESS THAN SOME OTHER CRITICAL SPEED [9], A SEPARATED FLOW (TERMED ANNULAR OR WAVY ANNULAR FLOW) IS POSSIBLE.

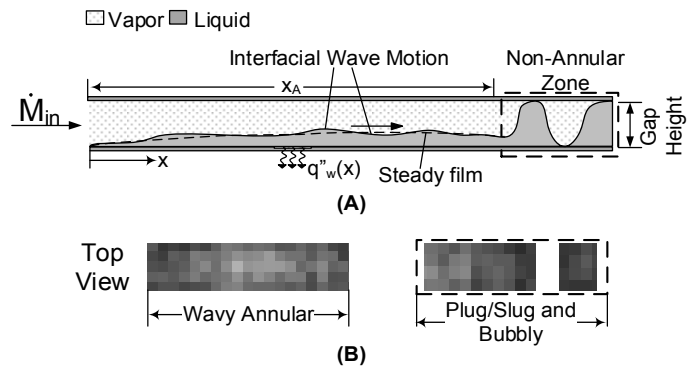


FIGURE 3: (A) SCHEMATIC OF FLOW TRANSITION FROM ANNULAR/STRATIFIED TO PLUG/SLUG FLOWS IN A MM-SCALE AND SUFFICIENTLY LONG CHANNEL CONDENSER WHOSE BOTTOM PLATE IS COOLED. (B) EXPERIMENTAL PHOTOGRAPHS ([4]) OF A TYPICAL REALIZATION.

The flow variables and fluid properties for the liquid and vapor phases of the condensing flows illustrated above are denoted with the subscript I (where $I = 1$ or L is for the liquid phase and $I = 2$ or V is for the vapor phase). In the description of low Mach number flow condensation in this paper, the fluid properties symbols for either of the two phases are: density ρ ,

dynamic viscosity μ , specific heat C_p and thermal conductivity k . Over the entire length of the condenser under consideration, the above fluid properties are modeled as approximate constants – though they take separate and different values for each of the two phases (subscripted by $I = 1$ or 2). Inlet velocity is parallel to the condenser plates (x -axis in Fig. 1) and its averaged magnitude at inlet is denoted by U_{in} , inlet pressure by p_{in} , and inlet temperature by $T_{sat}(p_{in})$ even if it is slightly superheated (this is because, as is well known in [22, 23], theory and experiments establish that 2-10°C superheat in the inlet vapor temperature lead to behavior very close to saturated vapor flows). The temperature fields in the interior of each phase are denoted by T_I , pressure fields by p_I , and the velocity fields by $\vec{V}_I \equiv u_I^p \hat{i} + v_I^p \hat{j}$ (where \hat{i} and \hat{j} are unit vectors along the x and y axes shown in Fig.1). The film thickness is denoted by Δ and the local interfacial mass flux per unit area (in $\text{kg/m}^2/\text{s}$) by \dot{m}^p . As noted earlier, the local average temperature at the x -location of the bottom condensing plate is $T_w(x) = T_{sat}(p_{in}) - \Delta T(x)$, where $\Delta T(x) > 0$ represents the local characteristic temperature-difference for the x -location. Different spatially varying steady wall temperature function $T_w(x)$ may arise from different “methods of cooling” for the condensing surface ([3]). The spatially averaged temperature $\overline{T_w} \equiv \int_0^L T_w(x) dx / L$ can be used to define a mean temperature difference $\overline{\Delta T} \equiv T_{sat}(p_{in}) - \overline{T_w}$. Under the conditions specified above, a particular “method of cooling” is defined by a particular function $\phi(x) \equiv \Delta T(x) / \overline{\Delta T}$. For all cooling methods that lead to a uniform condenser surface temperature $T_w(x)$, i.e. $T_w(x) = \overline{T_w}$ constant over $0 \leq x \leq L$, the “method of cooling” is said to be the same and is characterized by the constant function $\phi(x) = 1$. From here and henceforth, unless otherwise specified (as is typical of most studies), only those “methods of cooling” classes will be considered for which an assumption of approximate uniform wall temperature, i.e. $T_w(x) \cong \overline{T_w}$ or $\phi(x) \cong 1$, is adequate as far as development of the primary HTC correlations and flow-regime maps are concerned.

Later on we discuss an approach by which significant deviations from $\phi(x) \cong 1$ cases can still be adequately addressed with regard to spatial variation effects on flow variables (heat-flux or quality X) of interest. This is possible because quality based engineering HTC correlations that are developed (as discussed in section-3 of this paper) exhibit the feature that they themselves are not significantly affected by significant departures from the tentative modeling assumption of $\phi(x) \cong 1$.

When variations in local interfacial values of saturation temperature $T_{sat}(p_2^i)$ and heat of vaporization $h_{fg}(p_2^i)$ are allowed in computational simulations ([22, 23]) through computed variations in local x -dependent interfacial pressure p_2^i , it is found that - for applications with large values of steady inlet pressure p_{in} (typically in 50 – 1000 kPa range) - pressure differences over the channel are sufficiently small relative to the steady inlet pressure p_{in} . As a result, well-known approximations $T_{sat}(p_2^i) \cong T_{sat}(p_{in})$ and $h_{fg}(p_2^i) \cong h_{fg}(p_{in})$ are found to be adequate approximations for typical fluids and flows under consideration. For wavy interface annular/stratified

flows of interest, because of presence of liquid-vapor surface tension σ (at the representative temperature $T_{sat}(p_{in})$) in one of the critical interface conditions ([22, 23]), surface tension parameter σ is expected to be relevant – particularly in values of variables at locations where steady interfacial curvatures are large (e.g. σ is likely to be important ahead of or around the location $x \cong x_A$ in Fig. 3).

In Fig. 1, the length of the channel is denoted by L , the channel height by h , and channel width by w (with $h/w \ll 1$). The characteristic length h is used for non-dimensionalization of flow variables. The hydraulic diameters ($D_h \equiv 4A_c/P_w$, where A_c is the duct cross-section and P_w is the wetted perimeter) for characteristic length are also used and are to be defined and used differently for assessing heat-transfer rates through non-dimensional HTC (or Nusselt number) correlations available in the literature as well as for assessing vapor-phase turbulence through critical vapor-phase Reynolds number definitions available in the literature.

At any location x , the heat flow per unit area $q_w''(x)$ is determined by the flow geometry, the average inlet speed U_{in} (or inlet mass flow rate), relevant fluid properties of each phase (including saturation temperature and heat of vaporization), and the cooling conditions (as defined by the characteristic temperature difference $\overline{\Delta T}$ and the actual values of $\phi(x)$). Because heat flow rate from the nearly saturated vapor core to the interface can be ignored in comparison to: (i) the latent heat release rate at the interface, and (ii) the heat flow from the interface to the condensing surface; the vapor’s thermal conductivity and specific heat are not expected to be important in the determination of wall heat-flux. Therefore, the defining relationship between heat-flux $q_w''(x)$ and local HTC h_x is chosen to be:

$$\begin{aligned} q_w''(x) &\equiv h_x \{T_{sat}(p_{in}) - \overline{T_w}\} \\ &\equiv h_x \cdot \overline{\Delta T}, \end{aligned} \quad (1)$$

where, at most, the following list of variables are expected to affect the local HTC h_x :

$$\begin{aligned} h_x & \\ &\equiv h_x(x, U_{in}, \Delta T, \rho_1, \rho_2, \mu_1, \mu_2, C_{p1}, k_1, h_{fg}, |g_y|, \sigma) \end{aligned} \quad (2)$$

Similarly, because the length x_A of the annular regime is self-determined by the flow, it is expected that:

$$x_A \equiv x_A(U_{in}, \Delta T, \rho_1, \rho_2, \mu_1, \mu_2, C_{p1}, k_1, h_{fg}, |g_y|, \sigma) \quad (3)$$

Furthermore, it is commonly and correctly assumed in available empirical - and rather general (attempting to cover different flow-physics) - correlations ([12, 13]) that the form of the functions in Eqs. (1-2) depend on laminar or turbulent nature of the vapor and the liquid flows. What is often missed (as in [12]) is that, for mm-scale shear driven condensers, the shear driven liquid condensate motion is thin, slow, and nearly always laminar (discounting low amplitude interfacial turbulence restricted to the random nature of interfacial waves – that are typically found superposed on the steady laminar solutions). The adjoining near-interface vapor flow (with its streamlines bending

and piercing the interface (as shown in [16-18, 22, 23]) with an effective suction) is also laminar – even if the far-field vapor core is turbulent.

Either application of the well-known Pi-theorem ([24]) or consideration of the non-dimensional differential forms of the governing equations (see [16-18, 22, 23]) imply the following non-dimensional version of the dependencies given in Eqs. (2-3):

$$\text{Nu}_x \equiv \frac{h_x \cdot h}{k_1} = \text{Nu}_x|_h \quad (4)$$

$$= \widehat{f}_1 \left(\widehat{x}, \text{Re}_{in}, \text{Ja}, \text{Pr}_1, \frac{\rho_2}{\rho_1}, \frac{\mu_2}{\mu_1}, g_{nd}, \text{Su} \right) \quad (4)$$

$$\widehat{x}_A = \widehat{f}_2 \left(\text{Re}_{in}, \text{Ja}, \text{Pr}_1, \frac{\rho_2}{\rho_1}, \frac{\mu_2}{\mu_1}, g_{nd}, \text{Su} \right) \quad (5)$$

where \widehat{f}_1 and \widehat{f}_2 are unknown functions that are to be experimentally and/or theoretically/computationally determined. These functions may depend on: $\widehat{x} \equiv x/h$, $\widehat{x}_A \equiv x_A/h$, $\text{Nu}_x \equiv h_x \cdot h/k_1$, $\text{Re}_{in} \equiv \rho_2 U_{in} h/\mu_2$, $\text{Ja} \equiv c_{p1} \cdot \Delta T/h_{fg}(p_{in})$, $\text{Pr}_1 \equiv \mu_1 \cdot c_{p1}/k$, $\text{Su} \equiv \sigma \rho_2 h/\mu_2^2$, and $g_{nd} = |g_y| \rho_2^2 h^3/\mu_2^2$. Note Nu_x , Re_{in} , Ja , Su and g_{nd} are respectively called local Nusselt number, inlet Reynolds number, Jakob number, liquid Prandtl number, Suratman number, and a non-dimensional transverse gravity number.

Furthermore, for most applications of interest, condensate film thickness $\Delta(x)$ is found to be sufficiently small relative to h and one can typically ignore convection in the liquid film's differential form of energy equation (as in [7]). As a result, linear temperature variations in the condensate are known to be a very good approximation - both for wavy quasi steady and strictly steady flows ([22, 23]). This fact combines the aforementioned (in Eqs. (4-5)) separate dependences on Jakob (Ja) and liquid Prandtl (Pr_1) numbers to a single number Ja/Pr_1 . Also, as discussed in later sections, the transverse gravity parameter g_{nd} and surface-tension parameter Su , has a weak impact on h_x (except at $x \approx x_A$) and also on factors determining the lower bound of x_A (with impact being greater at $x > x_A$). Therefore, for flows of interests here, Eqs. (4-5) can be simplified to:

$$\text{Nu}_x \cong \widehat{f}_1 \left(\widehat{x}, \text{Re}_{in}, \frac{\text{Ja}}{\text{Pr}_1}, \frac{\rho_2}{\rho_1}, \frac{\mu_2}{\mu_1} \right) \quad (6)$$

$$\widehat{x}_A \cong x_A/h \cong \widehat{f}_2 \left(\text{Re}_{in}, \frac{\text{Ja}}{\text{Pr}_1}, \frac{\rho_2}{\rho_1}, \frac{\mu_2}{\mu_1}, g_{nd}, \text{Su} \right) \quad (7)$$

Furthermore, at any location x of a quasi-steady flow realization, it should be noted that mass balance for a liquid-vapor control volume between $x = 0$ and a location x in Fig. 1 can be written as:

$$\dot{M}_{in} \equiv \dot{M}_L(x) + \dot{M}_V(x) \quad (8)$$

where $\dot{M}_L(x)$ and $\dot{M}_V(x)$ are respectively cross sectional mass flow rates (kg/s) of the separated liquid/vapor flow. It is common practice to define vapor quality $X(x)$ as:

$$X(x) \equiv \dot{M}_V(x)/\dot{M}_{in} \quad (9)$$

Thus, from mass balance Eq. (9), one obtains

$$\dot{M}_L(x)/\dot{M}_{in} \equiv 1 - X(x) \quad (10)$$

Energy balance for the liquid-vapor control volume in Fig. 1 (which is of width Δx along the flow and depth w across the flow) is easily shown to yield (see [15]):

$$\dot{M}_{in} \cdot \frac{dX(x)}{dx} \cdot h_{fg} = -\{h_x \cdot \Delta T\} w \cdot \phi(x) \quad (11)$$

Using $\widehat{x} \equiv x/h$ and other introduced non-dimensional numbers, along with the assumption that the “method of cooling” is modeled by $\phi(x)$, it is easily shown that the non-dimensional version of Eq. (11) is:

$$\frac{dX(\widehat{x})}{d\widehat{x}} = -\text{Nu}_x \cdot \frac{\text{Ja}}{\text{Re}_{in} \cdot \text{Pr}_1} \cdot \frac{\mu_1}{\mu_2} \phi(\widehat{x}) \quad (12)$$

where $X(0) = 1$ but, because of a singularity (infinite value) in Nu_x correlations at $X \approx 1$, it is best to solve Eq. (12) with suitably chosen $\varepsilon \approx 0$ that require $X(\varepsilon) = X^*$, where X^* is close to 1 (say 0.99).

For the flow in Fig. 1, whether one uses experimental or computational approach to obtain the correlation for Nu_x and x_A/h in Eqs. (6-7), it is clear that the chosen correlations should be consistent with critical physics constraints - such as the satisfaction of mass, momentum, and energy balance equations (and, therefore, Eq. 12).

Substitution of the dependence in Eq. (6) in the energy-balance Eq. (12) makes it an explicit linear ordinary differential equation (ODE) which, when solved under the known condition of $X(\widehat{x} \cong 0) \cong 1$ and assumed $\phi(x) \cong 1$ condition, clearly yields the expected dependence:

$$X(\widehat{x}) = X \left(\widehat{x}, \text{Re}_{in}, \frac{\text{Ja}}{\text{Pr}_1}, \frac{\rho_2}{\rho_1}, \frac{\mu_2}{\mu_1} \right) \quad (13)$$

3. FORMS OF DEPENDENCES ASSUMED IN THE LITERATURE FOR OBTAINING NON-DIMENSIONAL HTC CORRELATIONS AND FLOW-REGIME TRANSITION MAPS

The fundamental non-dimensional forms of correlations for HTC (h_x) applicable to annular/stratified shear driven condensing flows, as given by Eq. (4) or Eq. (6), is proposed in the literature (e.g. see relevant correlations of Shah [20], Kim and Mudawar [12], Wang [21], Dobson and Chato [[19]], etc.) in forms that are equivalent to:

$$\text{Nu}_x|_{D_h} \equiv h_x \cdot D_h / k_1 = \widehat{f}_n \left(X(\widehat{x}), \text{Re}_{in}|_{D_h}, \frac{\rho_2}{\rho_1}, \frac{\mu_2}{\mu_1}, \text{Su}|_{D_h} \right) \quad (14)$$

where $0 \leq X \leq 1$ and function \widehat{f}_n is implicitly defined by the available correlations ([12, 19-21]) with hydraulic diameter D_h replacing h in the earlier definitions for Re_{in} and Su . Note that the tube-diameter D equals D_h for shear-driven in-tube condensation.

The D_h definition, as far as heat transfer rates are concerned, is $D_h \cong 4h$ for the single-sided condensing flow in Fig. 1, and $D_h \cong 2h_{II}$ for the double-sided condensing flow case in Fig. 2B. With all other flow and fluid parameters kept identical between the two channel flows in Fig. 1 and Fig. 2, use of $h_{II} = 2h$ in Fig. 2B doubles the inlet mass flow rate with respect to the flow in Fig.1 (as U_{in} remains the same for the two cases) and makes the condensing flow in each of its symmetric halves approximately the same as in Fig. 1. This leads to the expectation that, under these conditions, at the same physical distance x , the local heat-flux $q_w''(x)$, and the local HTC h_x are going to be the same and, therefore, the correlations for the two flow situations should satisfy (and relate to the definition in Eq. (14)) through the relationship:

$$\begin{aligned} Nu_x|_{D_h=2h} &\cong \frac{1}{2} Nu_x|_{D_h=4h}, \\ \text{i. e. } Nu_x|h &\cong \frac{1}{4} Nu_x|_{D_h=4h} \end{aligned} \quad (15)$$

If curvature effects could be ignored (which is questionable for mm-scale condensers), an in-tube (inner diameter D) shear driven condensing flow would be equivalent to the flow in Fig. 2B (with width $w = \pi D/2$) and one would expect (in addition to Eq. (15)):

$$Nu_x|h \cong \frac{1}{4} Nu_x|_{D_h=4h} \cong \frac{1}{4} Nu_x|_{D_h=D} \quad (16)$$

Continuing to use $\hat{x} \equiv x/h$ while repeating the arguments for Eq. (12) - with the help of $Nu_x|_{D_h}$ and $Re_{in}|_{D_h}$ definitions in Eq. (14) instead of the $Nu_x|h$ and $Re_{in}|h$ definition in Eq. (4), one obtains:

$$\frac{dX(\hat{x})}{d\hat{x}} = - Nu_x|_{D_h} \cdot \frac{Ja}{Re_{in}|_{D_h} \cdot Pr_1} \cdot \frac{\mu_1}{\mu_2} \phi(\hat{x}) \quad (17)$$

Using vast quantities of existing experimental data for mm-scale tubes and square/rectangular ducts ([12]), simulation capabilities for channels ([16-18, 22, 23]), and experimental data ([3, 4]) for channels (i.e. small aspect ratio rectangles with $h/w \ll 1$), this paper intends to propose HTC correlations and test the equivalence efficacy of Eqs. (15-17).

Substitution of Eq. (14) in the one-dimensional energy balance Eq. (17) makes it an implicit non-linear ordinary differential equation in $X(\hat{x})$ - which is solvable (despite the singularity at $\hat{x} \cong 0$) and yields an explicit dependence of quality X on non-dimensional downstream distance \hat{x} . It is again clear that the solution gives the quality X in a dependence whose form is consistent with the one in Eq. (13). Clearly any substitution of the resulting correlation for quality $X(\hat{x})$ (obtained/developed by experimental and/or theoretical/computational approach) in the original Nusselt number dependence of Eq. (14) implies that the resulting argument list is equivalent to the original fundamental argument list in Eq. (4). However, this implication is not the same as the one in which one obtains an explicit fundamental

Nusselt-number and quality $X(\hat{x})$ correlations in their respective fundamental forms (Eq. (4) and Eq. (13)) and then shows that these can be combined to obtain the popular/conventional form exemplified by Eq. (14). An argument implying this is approximately true is given in section-5 of this paper - and although this justifies the literature's approach embodied in Eq. (14), better and more accurate correlation approaches may retain Ja/Pr_1 dependence.

Additionally, semi-empirical flow regime maps are available in the literature. They are either used indirectly for condensing flows as they are originally based on flow regimes observed inside large diameter tubes with air-water type shear/pressure driven adiabatic flows (Baker [9], Taitel and Dukler [8], Coleman and Garimella [10], etc.) or they are directly developed/used on the basis of consideration of shear/pressure driven condensing flows (e.g., for millimeter scale channels, see transition criteria of Kim and Mudawar [12], etc.). The one in [12] and our own theoretical/computational results in [16-18] hold the promise of identifying the annular/stratified to plug/slug transition of interest here by developing explicit dependence in the form given by Eq. (7). To show that this promise can be realized, it is to be noted that semi empirical flow regime maps are typically obtained from a hypothesis that is tacitly assumed for condensing flows because, perhaps, the hypothesis is rather obvious for air-water flows. The hypothesis states that all the flow-regime transitions (annular to slug/plug, plug/slug to bubbly, annular to dispersed-liquid, etc.) may be marked by various curves in the parameter space of $\{X, Re_{in}, \rho_2/\rho_1, \mu_2/\mu_1, Su, g_{nd}\}$. These various curves can be denoted as X_{cr_i} (say $i = 1$ for annular/stratified to plug/slug, $i = 2$ for wavy annular to dispersed-liquid, and $i = 3$ for plug/slug to bubbly, etc.) and can be obtained as curves in the above identified parameter space. Such transition-marking curves can be expressed as a single curve or a combination of single curves in the form:

$$X_{cr_i} = X_{cr_i} \left(Re_{in}, \frac{\rho_2}{\rho_1}, \frac{\mu_2}{\mu_1}, Su, g_{nd} \right) \quad (18)$$

where the subscript i in X_{cr_i} takes the values of 1,2,3, etc. The curve X_{cr_1} which marks the transition from annular/stratified to plug/slug is of primary interest here.

3.1 Examples of Semi-Empirical HTC (h_x) Correlations and their Approximate Equivalence to the Representation in Eq. (14)

For shear driven condensing flows (with h as in Fig.1 and $D_H \cong 4h$), there are well known correlations in [12, 19-21], etc. These correlations are available in the literature and are well summarized and assessed in a recent article of Kim and Mudawar ([12]). For reasons of brevity, only Nu_x correlation from Kim and Mudawar ([12]) is primarily considered in this paper and is shown to be approximately equivalent to the standardized structure of Eq. (14). A cursory look at these correlations may appear to suggest that they use different non dimensional parameters such as: Lockhardt Martinelli Parameter X_{tt} that explicitly depends on quality X , a two-phase multiplier

ϕ_g representing a certain ratio of well-defined pressure gradients, etc. (see Tables 2 and 4 in [12]). This paper intends to show that if one substitutes the acceptable correlations in one-dimensional energy balance (Eq. (17)) and one solves the resulting ODE (subject to $X(\epsilon) = X^*$); one can computationally obtain explicit form of $X(\hat{x})$ and $Nu_x(\hat{x})$ – and such dependences are effectively characterized by the arguments list in Eq. (6), and Eq. (13).

The HTC correlation recently proposed by Kim and Mudawar ([12]) is:

$$Nu_{x|D_h} \equiv \frac{h_x \cdot D_h}{k_1} = 0.048 Re_1^{0.69} Pr_1^{0.34} \left(\frac{\phi_g}{X_{tt}} \right), \quad (19)$$

where X_{tt} and ϕ_g are defined in Table 4 of [12]. Clearly, this correlation does not explicitly show any dependence on the thermal boundary condition as uniform surface temperature class of $\phi(x) \cong 1$ is considered adequate though, if needed, $\phi(x) \neq 1$ may still be used in Eq. (17).

For a representative condensing flow of FC-72 vapor, use of FC-72 thermodynamic properties at $p_{in} = 100$ kPa allows one to specify the raw argument list through set **A** $\equiv (U_{in}, h, \rho_1, \rho_2, \mu_1, \mu_2, c_{p1}, k_1, h_{fg}, \Delta T, \sigma) = (1 \text{ m/s}, 0.002 \text{ m}, 1603 \text{ kg/m}^3, 13.06 \text{ kg/m}^3, 0.000494 \text{ kg/m-s}, 1.16e-5 \text{ kg/m-s}, 1.142 \text{ kJ/kg-K}, 0.07041 \text{ W/m-K}, 83.54 \text{ kJ/kg}, 15 \text{ }^\circ\text{C}, 0.008329 \text{ N/m})$ to evaluate Eq. (19) and substitute it in the ODE Eq.(17). One then obtains the ODE’s numerical solution on MATLAB. This specific flow situation is equivalently characterized by the non-dimensional parameters list/set **NA** $\equiv (Re_1 = Re_{in|D_h}, Ja/Pr_1, \rho_2/\rho_1, \mu_2/\mu_1, Su) = (9006, 0.0307, 0.008, 0.0234, 6.44e6)$. For this correlation and flow situation, the $Nu_{x|D_h} - X$ variation and $X(\hat{x})$ are respectively shown in Figs. 4A and 4B (for $0 \leq \hat{x} \leq 100$).

Next one artificially changes fluid properties and FC-72 condensing flow situation from their representative values of set **A** to a new raw argument list given by set **A*** $\equiv (U_{in}, h, \rho_1, \rho_2, \mu_1, \mu_2, c_{p1}, k_1, h_{fg}, \Delta T, \sigma) = (0.833 \text{ m/s}, 0.0024 \text{ m}, 1923.6 \text{ kg/m}^3, 15.672 \text{ kg/m}^3, 5.928e-4 \text{ kg/m-s}, 1.39e-5 \text{ kg/m-s}, 1.142 \text{ kJ/kg-K}, 0.08449 \text{ W/m-K}, 83.54 \text{ kJ/kg}, 15 \text{ }^\circ\text{C}, 0.008329 \text{ N/m})$ but the values of non-dimensional parameters: set **NA** $\equiv (Re_{in}, Ja/Pr_1, \rho_2/\rho_1, \mu_2/\mu_1, Su) = (9006, 0.0307, 0.008, 0.0234, 6.44e6)$ are kept the same. The resulting $Nu_x - X$ curve for this second situation, as shown in Figs. 4A-B, remains approximately the same as the first situation. This verifies that Kim and Mudawar correlation (and perhaps some other “good” correlations) has effectively the same dependence as the fundamental one described in Eq. (14).

Despite the above feature, a fundamental limitation of such empirical correlations are that they deal directly with the raw arguments list/set **A** rather than the one associated with the non-dimensional parameters list/set **NA**. In an attempt to cover a range of non-dimensional values towards overcoming this limitation, one typically considers/specifies a set of working fluids, hydraulic diameters, and operating conditions to first

define the range of values of interest for the argument list/set **A**. For example, this paper chooses/defines its argument list/set **A** through the choices given in Table-1.

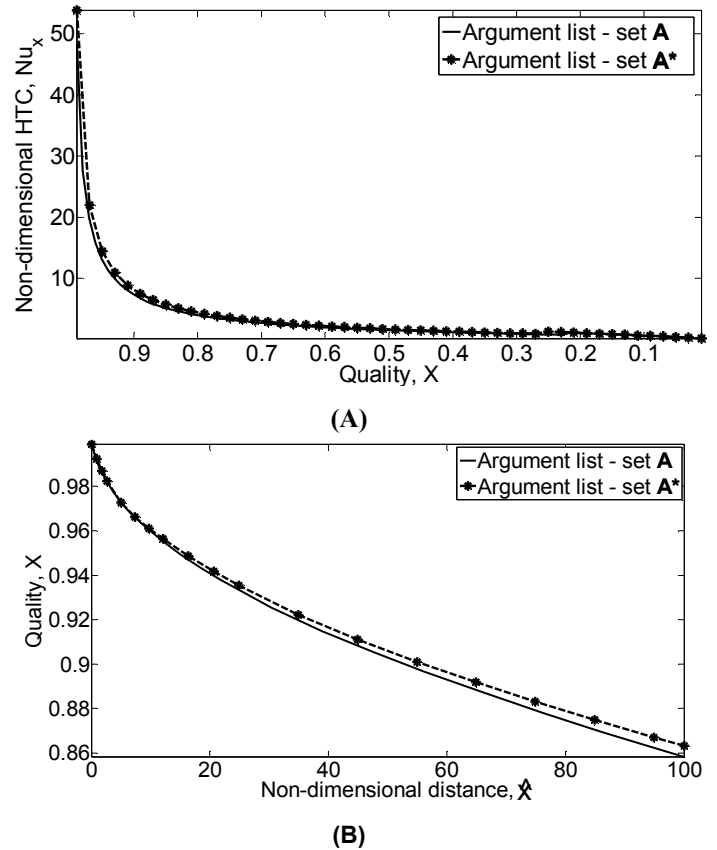


FIGURE 4: FOR THE REPRESENTATIVE CONDENSING FLOW OF FC-72 SPECIFIED BY SET “NA,” THE FIGURES SHOW: (A) NUSSELT NUMBER Nu_x VERSUS QUALITY X , and (B) QUALITY X VERSUS NON-DIMENSIONAL DISTANCE \hat{x} VARIATIONS.

As a result of the above choice for the range of flows, one can typically obtain heat transfer coefficient h_x data (experimentally or computationally) only at a set of discrete points in the $\{\hat{x}, Re_{in}, Ja/Pr_1, \rho_2/\rho_1, \mu_2/\mu_1, Su\}$ space of Eq. (4) or $\{X, Re_{in}, \rho_2/\rho_1, \mu_2/\mu_1, Su\}$ space of Eq. (14). Such discrete point-wise raw variable data, when combined with experimental challenges in accessing the desired range, often lead to discrete point-wise data of non-dimensional values that are not conducive to developing reasonably accurate empirical correlations. For example the choice in Table-1 has limited experimental accessibility in the associated $\{Re_{in}, Ja/Pr_1, \rho_2/\rho_1, \mu_2/\mu_1, Su, g_{nd}\}$ space described in Table-2.

TABLE-1: RANGE OF FLUIDS AND FLOW CONDITIONS CONSIDERED FOR FLOW IN FIG. 1

Working fluids	FC-72	R113	R113	R134a
Inlet Pressure (kPa)	100	25	225	150
Saturation temperature (°C)	55.94	11.1	73.86	-17.15
Hydraulic Diameter ($h = 0.002$ m)	2h	2h	2h	2h
Transverse Gravity	$0 \leq g_y \leq g$			
Inlet Vapor Speed (U) (m/s)	0.35 – 9.79	2.07 – 57.16	0.35 – 9.79	0.54 – 14.9
ΔT (°C)	2.93 – 12.30	8.69 – 36.50	2.25 – 9.45	3.45 – 14.45

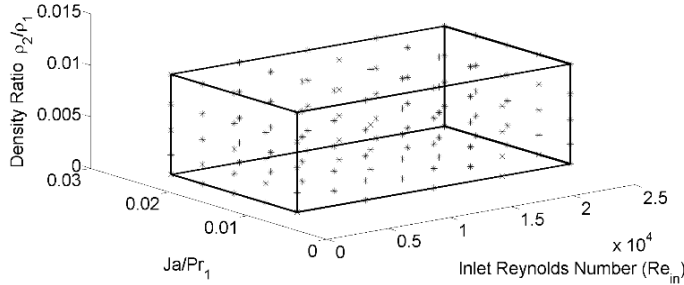
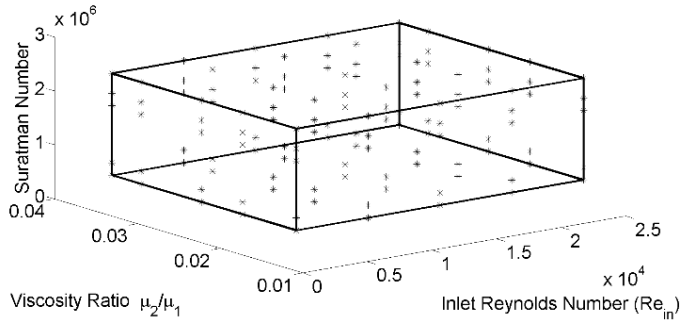
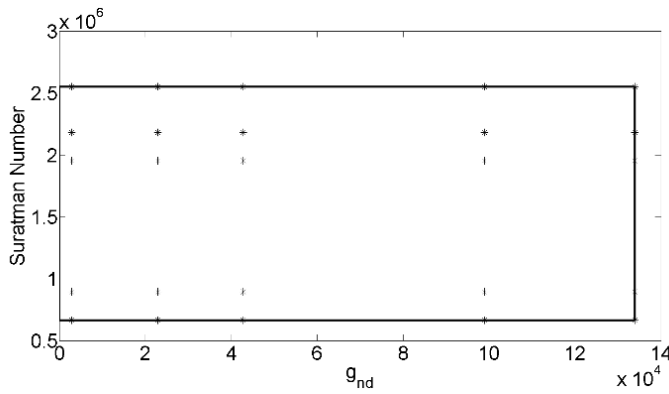

(A)

(B)

(C)

FIGURE 5: FOR CORRELATIONS DEVELOPED IN THIS PAPER, THE $\{Re_{in}, Ja/Pr_1, \rho_2/\rho_1, \mu_2/\mu_1, Su, g_{nd}\}$ SPACE THAT IS COVERED IS VISUALIZED THROUGH: (A) A THREE-DIMENSIONAL $\{Re_{in}, Ja/Pr_1, \rho_2/\rho_1\}$ SPACE, (B) A THREE-DIMENSIONAL $\{Re_{in}, \mu_2/\mu_1, Su\}$ SPACE, AND (C) A TWO-DIMENSIONAL $\{g_{nd}, Su\}$ SPACE.

In this paper, by combining experimental and computational approaches, the range in Table-2 is more judiciously covered for any chosen boxed zone (dashed lines in Fig. 5A-C) – e.g. including its boundaries and interior (center, diagonal, etc.) - to develop meaningful correlations for a chosen range.

TABLE-2: RANGE OF NON-DIMENSIONAL PARAMETERS ASSOCIATED WITH TABLE-1

800	\leq	Re_{in}	\leq	23000
0.005	\leq	Ja/Pr_1	\leq	0.021
0.0013	\leq	ρ_2/ρ_1	\leq	0.011
0.012	\leq	μ_2/μ_1	\leq	0.0343
$6.63 * 10^5$	\leq	Su	\leq	$2.55 * 10^6$
0	\leq	g_{nd}	\leq	$1.33 * 10^5$

Though the boxed zone can be extended or several such boxed zones (e.g. see water condensation cases in [15]) may be considered, this paper's focus is for the well-defined range in Table-2.

3.2 Examples of Semi-Empirical Flow-Regime Maps and their Typical Representation

Shear driven annular condensing flows' experimental realization at low to moderate inlet Reynolds number Re_{in} (or inlet mass-flux G , as in [12]) typically show (see Carey [6], Kivisalu et al. [3], Kim and Mudawar [12]) transitions indicated in Fig. 3 i.e. annular/stratified to plug/slug to bubbly. Similar transitions are indicated in large diameter adiabatic air/oil flow experiments of Baker ([9]) whose flow-regime map, though not properly non-dimensional, is typically considered along with other popular adiabatic flow-regime maps (Taitel and Dukler [8], etc.) - even for condensing flows ([6]). This is based on the assumption that the instabilities associated with the transition curves in these maps are mechanical in nature - i.e. only mass and momentum balances are involved once energy Eq. (12) yields the quality $X(\hat{x})$. Furthermore, maps or transition criteria specific to condensing flows ([12], etc.) exist. It is found (in [15]) that Taitel and Dukler ([8]) map, though properly non-dimensional, does not relate to mm-scale condensing flow transitions observed in [3] and [12] – perhaps as a result of very large diameter tubes and different orientations considered in the creation of the map. Similarly, in [16], we find that, after proper non-dimensionalization, Baker-map ([9]) does yield qualitatively similar transitions as those observed in mm-scale

shear driven condensing flows (as in Fig. 3). Despite this, because of the larger diameter tubes (several cms) involved, the trends of the transition curves are quite different than those directly obtained for mm-scale condensers – either in experiments ([3]) or through theory and computations (results discussed later on in this paper on the basis of our CFD-based stability results of [16-18]). For the above reasons, in this section, we primarily discuss annular/stratified to plug/slug empirical transition criteria of Kim and Mudawar ([12]).

3.2.1 Kim and Mudawar Criteria for Annular to Plug/Slug Transition

Using FC-72 condensing flow data in horizontal mm-scale tubes and square/rectangular cross-section ducts, Kim and Mudawar ([12]) provide an annular to plug/slug transition criteria and correlation. Their criteria of $We^* = 7X_{tt}^{0.2}$ at transition, with definitions of We^* and X_{tt} , is more fully defined in [12]. This annular ($We^* > 7X_{tt}^{0.2}$) to non-annular plug/slug ($We^* < 7X_{tt}^{0.2}$) transition criteria is used for the specific cases of pure FC-72 condensation ($D_H = 8$ mm and $p_{in} = 100$ kPa) considered in Fig. 6. The results (for a relevant range of $Re_{in|Dh}$) for fixed values of $\{\rho_2/\rho_1, \mu_2/\mu_1, Su\}$, are depicted in the $Re_{in|Dh} - X$ plane of Fig. 6.

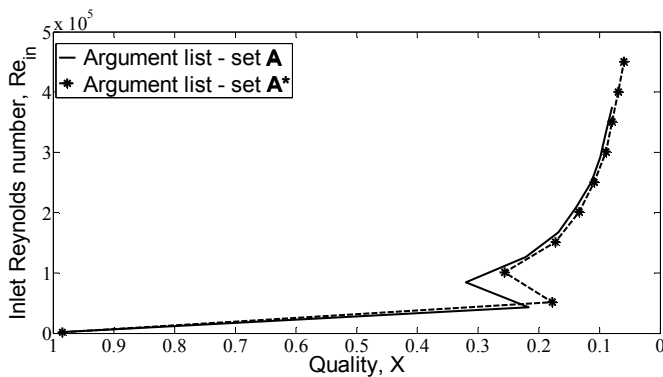


FIGURE 6: THE FIGURE ABOVE PRESENTS A SPECIFIC USE OF THE KIM AND MUDAWAR [12] CRITERIA FOR ANNULAR TO PLUG/SLUG TRANSITIONS FOR CONDENSATION OF PURE FC-72 ($D_h = 8$ mm AND $p_{in} = 100$ kPa) AND PRESENTS THE TRANSITION CRITERIA IN THE $Re_{in} - X$ PLANE FOR FIXED VALUES OF $(Ja/Pr_1, \rho_2/\rho_1, \mu_2/\mu_1, Su, g_{nd}) = (0.0307, 0.008, 0.0234, 6.44e6, 6.36e6)$.

Again as in Fig. 4, when one artificially changes fluid properties for a representative FC-72 condensing flow situation from raw argument set A to set A* in a way that the non-dimensional parameters set NA remains the same, the resulting $Nu_x - X$ curve for this second situation remains approximately the same as before. This fact is shown in Fig. 6. This verifies that Kim and Mudawar transition criteria ([12]) has effectively the same dependence as the fundamental one described in Eq. (4). However, this does not mean that the criteria has as much experimental support as their $Nu_{x|Dh}$ correlations. This is

because experimental data for x_A is limited (i.e., not measured for all the experimental runs cited in [12]).

4. COMPUTATIONAL APPROACH FOR ANNULAR SHEAR DRIVEN CONDENSING FLOW REGIME

Steady and unsteady solutions are computationally obtained and correlated to propose non-dimensional HTC (h_x) and length x_A estimates through their dependences ascertained in the format of Eqs. (4-5). The computational approach currently limits itself to estimates of Nu_x applicable to steady and wave-free cases (i.e. quasi-steady and low-amplitude waves) – though an empirical correction approach for wave effects is described. In section 5, it is shown that the proposed correlations in the format of Eqs. (4-5) can also be re-cast in the frequently used correlation formats given in Eqs. (14-15).

The governing equations for the computational approach is described in ([16-18, 22, 23]) whereas the more recent and successful steady/unsteady simulation algorithm are described in ([16-18]).

The simulation capability uses an approach of separately solving, on COMSOL, the unsteady liquid and vapor domain governing equations over their respective domains that result from an assumed "sharp" interface location. Accurately locating the interface at time "t," the approach tentatively treats the two domains to be "fixed" over a short time interval of time $[t, t+\Delta t]$. The interface location for time "t+ Δt " is then iteratively relocated by tracking the interface with the help of numerical solution of its evolution equation (which is obtained from one of the interface conditions [16-18, 22]) on MATLAB. This procedure employs a moving grid that takes into account the nature of wave propagation on the interface. Concurrently, the approach solves the unsteady liquid and vapor domain governing equations while suitable values of interfacial variables (speeds, stresses, temperatures, etc.) are imposed at the interface as boundary conditions. Later on, these assumed interfacial values of the flow variables are iteratively changed in the computations until the convergence towards satisfying all the remaining unsteady and well known interface conditions [16-18]. COMSOL's fluid flow and heat transfer modules are used for separately solving the liquid and vapor domain governing equations in the interior while the two solutions' are made to talk to one another, along with judicious but concurrent interface relocations, with the help of algorithms (see [16-18]) implemented on MATLAB (that links with COMSOL). Interface evolution equation is a wave equation which is solved (with the help of the well-defined characteristics equation underlying this problem) with 4th order accuracy in time. This kind of unique approach ensures accurate prediction of interface location and interface variables towards accurate satisfaction of all the time-varying interface conditions.

The approach and solutions in [16-18] are aided by improvements in implementation schemes relative to the ones described in our earlier papers ([22, 23]). As far as obtaining and correlating solutions for h_x and x_A are concerned, the signatures of instability that determines x_A in Fig. 3 is first identified through unsteady simulations and next related to its signature in the energy transfer mechanisms and flow variables associated

with the steady solutions. The h_x , x_A , etc. values obtained from the 2-D solution method and aided by a much faster 1-D solution technique described in [7], are correlated over the parameter space described in Table-2 and Fig. 5.

Consistency of the steady solutions obtained from the two independent approaches (2-D solver and 1-D solver) are shown in [7] and their consistency with gravity driven and shear driven flows' experimental results are respectively shown in [7] and [16, 17].

It suffices here to note that all the physical variables (in SI units unless mentioned otherwise) mentioned in the earlier paragraph can be non-dimensionalized. Furthermore non-dimensional form of the governing equations are considered by introducing the following non-dimensional variables ([16-18]):

$$\begin{aligned} \{x, y, \Delta, u_1^p, \dot{m}^p\} &\equiv \{L\hat{x}, L\hat{y}, L\delta, U_{in}u_1, \rho_1 U_{in}\dot{m}\} \\ \{v_1^p, T_1, p_1\} &\equiv \{U_{in}v_1, \Delta T\theta_1, p_{in} + \pi_1 \rho_1 U_{in}^2\} \end{aligned} \quad (20)$$

In Eq. (20) above \hat{x} , \hat{y} , δ , u_1 , \dot{m} , v_1 , θ_1 and π_1 are the non-dimensional forms of $x, y, \Delta, u_1^p, \dot{m}^p, v_1^p, T_1^p, p_1$. The governing equations and solutions for condensation of saturated vapor for the flow in Fig.1 are reconsidered after their non-dimensionalization through Eq. (20). The steady solutions indicate that thin liquid condensate flows under negligible effects of the convection term in the differential form of the condensate energy equation. Under this approximation the non-dimensional governing equations ([16-18, 22, 23]) clearly indicate the significance of the following non-dimensional parameters (some have been defined earlier):

$$\left\{ \text{Re}_{in}; \frac{\text{Ja}}{\text{Pr}_1}, \frac{\rho_2}{\rho_1}, \frac{\mu_2}{\mu_1}, \text{Fr}_y^{-2} \equiv \frac{|g_y|h}{U^2}, \text{We} \equiv \frac{\rho_2 U^2 h}{\sigma} \right\} \quad (21)$$

For the ‘‘black-box’’ empirical approach recommended for developing correlations within structures proposed in Eqs. (4-5), or Eq. (14) and Eq. (18), it is convenient to restrict inertia effects associated with the inlet mass flow rate to the inlet Reynolds number Re_{in} . It was for this reason Suratman number $\text{Su} \equiv (\sigma \rho_2 h / \mu_2^2)$ and transverse gravity number $g_{nd} \equiv (\rho_2^2 |g_y| h^3 / \mu_2^2)$ were introduced in the earlier section. Though the parameters in Eq. (21) more closely control the actual flow physics, the observation that $\text{We} \equiv \text{Re}_{in}^2 / \text{Su}$ and $g_{nd} \equiv \text{Fr}_y^{-2} \cdot \text{Re}_{in}^2$ allows one to see the equivalence between the parameter set in Eq. (21) with the one used earlier and given below:

$$\left\{ \text{Re}_{in}; \frac{\text{Ja}}{\text{Pr}_1}, \frac{\rho_2}{\rho_1}, \frac{\mu_2}{\mu_1}, \text{Su}, g_{nd} \right\} \quad (22)$$

The results given here and elsewhere [15-16] indicate insignificant impact of transverse gravity (through g_{nd}) on $\text{Nu}_x|_h$ but somewhat more significant impact on \hat{x}_A . These investigations [6, 16-18, 22-23] also establish that, for mm-scale condensers, the approximate argument list in Eqs. (6-7) is well supported by rigorous steady and unsteady solutions for shear driven annular/stratified flows.

5. RESULTS AND DISCUSSION

5.1 Computationally Obtained Values for Nu_x (or h_x), Quality $X(\hat{x})$, and Length \hat{x}_A along with their Correlations and Assessments

Steady solutions of the full 2-D governing equations were obtained in the parameter space defined by Table-2 and Fig. 5. It was found that the presence or absence of transverse gravity has negligible effects on steady solutions and associated heat-transfer rates (i.e. $\text{Nu}_x = \text{Nu}_x|_{0g} \cong \text{Nu}_x|_{1g}$). As discussed in [16-18], unsteady solutions based on onset of instability analyses yield the length of the annular zone $\hat{x}_A \equiv x_A/h$ which is somewhat affected by the presence or absence of transverse gravity. Furthermore, the signature of the onset of instability (associated with annular to plug/slug transitions) can be approximately identified/correlated ([16-18]) with the steady solutions' features dealing with spatial variations in mechanical energy transfer mechanisms and characteristic speeds/wave speeds.

Using natural log of the computed values of variables (both by 2-D and 1-D solvers) on either side of Eqs. (6-7) and employing linear regression with least square fits ([25]), the following correlations (with 5.7% average error for Nu_x) are obtained:

$$\begin{aligned} \text{Nu}_x &= 0.113 \hat{x}^{-0.433} \text{Re}_{in}^{0.503} \left(\frac{\text{Ja}}{\text{Pr}_1} \right)^{-0.308} \left(\frac{\rho_2}{\rho_1} \right)^{-0.537} \left(\frac{\mu_2}{\mu_1} \right)^{0.443} \end{aligned} \quad (23)$$

Based on the steady and unsteady analyses ([16-18]), the length of annular regime in absence of transverse gravity is identified by $\hat{x}_A|_{0g}$ and in the presence of transverse gravity is identified by $\hat{x}_A|_{1g}$. Through the analyses, an approximate value for the difference between the two lengths is correlated with measured features of the steady solution distances given by \hat{x}^* and $\Delta\hat{x}_{Cr}$. The relationship among $\hat{x}_A|_{0g}$, $\hat{x}_A|_{1g}$, \hat{x}^* and $\Delta\hat{x}_{Cr}$ is given in Eqs. (24-25). The actual values of $\hat{x}_A|_{0g}$ or $\hat{x}_A|_{1g}$, though somewhat uncertain because of the inherent behavior of a transition zone, are identified by a careful analysis of the unsteady CFD simulation tool results and is reported in [16-18]. A good estimate is given by:

$$\hat{x}^* \leq \hat{x}_A|_{0g} \leq \hat{x}^* + \beta \Delta\hat{x}_{Cr} \quad (24)$$

$$\text{and } \hat{x}_A|_{1g} \cong \hat{x}_A|_{0g} + \tilde{\beta} \Delta\hat{x}_{Cr} \quad (25)$$

It is typically found that $\beta \cong 0$ in Eq. (24), i.e. $\hat{x}_A|_{0g} \cong \hat{x}^*$ and $\tilde{\beta} \cong 1$ in Eq. (25), i.e. $\hat{x}_A|_{1g} \cong \hat{x}_A|_{0g} + \Delta\hat{x}_{Cr}$.

Correlations for $\hat{x}_A|_{0g}$ (with 6.433 % average error) and $\hat{x}_A|_{1g}$ (with 5.791 % average error) are presented below through Eqs. (26-27).

$$\begin{aligned} \hat{x}_A|_{0g} &= (0.0155 *) \text{Re}_{in}^{0.9616} \left(\frac{\text{Ja}}{\text{Pr}_1} \right)^{-1.1859} \left(\frac{\rho_2}{\rho_1} \right)^{0.4425} \left(\frac{\mu_2}{\mu_1} \right)^{0.3} \end{aligned} \quad (26)$$

$$\hat{x}_A|_{1g} = 2.9413 * Re_{in}^{0.8514} \left(\frac{Ja}{Pr_1}\right)^{-2.1714} \left(\frac{\rho_2}{\rho_1}\right)^{1.031} \left(\frac{\mu_2}{\mu_1}\right)^{1.6366} \quad (27)$$

Recall that the thin condensate film flow approximations (see [22, 23]) yield:

$$q''_w(x) \cong k_1 \frac{\Delta T}{\Delta(x)} \equiv h_x \cdot \Delta T \quad (28)$$

$$X(x) = \frac{\dot{M}_v(x)}{\dot{M}_{in}} = 1 - \frac{\dot{M}_L(x)}{\dot{M}_{in}} \cong 1 - \frac{Ja}{Re_{in} \cdot Pr_1} \cdot \frac{\mu_1}{\mu_2} \left[\int_0^{\hat{x} \equiv x/h} Nu_x d\hat{x} \right] \quad (29)$$

Using Eqs. (28-29), it is easy to show that the reported correlations in Eqs. (23-25) are consistent with the following correlations for the non-dimensional film thickness $\delta(x) \equiv \Delta(x)/h$ and quality $X(\hat{x})$:

$$\delta(\hat{x}) \cong 8.849 \hat{x}^{0.433} Re_{in}^{-0.503} \left(\frac{Ja}{Pr_1}\right)^{0.308} \left(\frac{\rho_2}{\rho_1}\right)^{0.537} \left(\frac{\mu_2}{\mu_1}\right)^{-0.443} \quad (30)$$

$$X(\hat{x}) \cong 1 - 0.81 \hat{x}^{0.73} Re_{in}^{-0.64} \left(\frac{Ja}{Pr_1}\right)^{1.02} \left(\frac{\rho_2}{\rho_1}\right)^{-0.33} \left(\frac{\mu_2}{\mu_1}\right)^{-0.86} \quad (31)$$

Substitution of $\hat{x} = \hat{x}_A$, with $\hat{x}_A = \hat{x}_A|_{0g}$ coming from the appropriate correlation in Eq. (26), into Eq. (29) above yields one of the relationships described in Eq. (18). For example, one gets:

$$X(\hat{x}_A|_{0g}) \equiv X_{cr-1}|_{0g} \left(Re_{in}, \frac{\rho_2}{\rho_1}, \frac{\mu_2}{\mu_1}, \frac{Ja}{Pr_1}, Su, g_{nd} \right) \cong 1 - 0.038 Re_{in}^{0.059} \left(\frac{Ja}{Pr_1}\right)^{0.16} \left(\frac{\rho_2}{\rho_1}\right)^{-0.006} \left(\frac{\mu_2}{\mu_1}\right)^{-0.647} \quad (32)$$

The dependence on Ja/Pr_1 term in Eq. (32) is weak – because its value ranges from 0.46 to 0.60 (see Ja/Pr_1 range in Table-2) – and one can approximately replace it by the form used in the literature and described in Eq. (18). This more approximate form is:

$$X(\hat{x}_A|_{0g}) \equiv X_{cr-1}|_{0g} \left(Re_{in}, \frac{\rho_2}{\rho_1}, \frac{\mu_2}{\mu_1}, Su, g_{nd} \right) \approx 1 - 0.0204 Re_{in}^{0.059} \left(\frac{\rho_2}{\rho_1}\right)^{-0.006} \left(\frac{\mu_2}{\mu_1}\right)^{-0.647} \quad (33)$$

For $\hat{x}_A|_{1g}$, correlations similar to the ones in Eqs. (32-33) can be obtained and reported – and this is done elsewhere ([16, 17]). Using X_{cr-1} values for identifying the annular to plug/slug transition curve for FC-72 condensation at $Ja/Pr_1 \cong 0.0256$, $\rho_2/\rho_1 \cong 0.008$, $\mu_2/\mu_1 \cong 0.0234$, $Su \cong 1.61e6$, and $g_{nd} \cong 9.95e4$ or $g_{nd} = 0$, transition curves are plotted in the $Re_{in} - X$ plane of Fig. 7. Thus, in Fig. 7, one obtains another

estimate (this time by a theoretical/computational approach) – besides those obtained from the empirical criteria of Kim and Mudawar ([12]). The differences between theoretical/computational and Kim and Mudawar are discussed in [15-17]. It suffices to note that: (i) the differences are not entirely accounted by differences in curvature effects (with aspect ratio $AR \equiv h/w$, $AR \approx 0$ and $AR \approx 1$), and (ii) our theoretical/computational estimates are supported by our $AR \approx 0$ experimental results of [3-4].

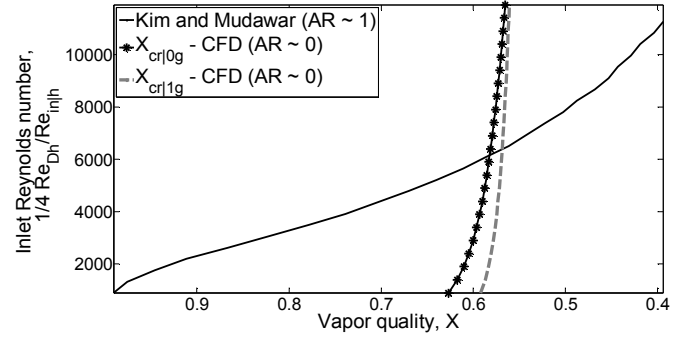


FIGURE 7: THE FIGURE PRESENTS CFD-PREDICTED AND KIM AND MUDAWAR [12] CRITERIA PREDICTED ANNULAR TO PLUG/SLUG TRANSITIONS CURVES FOR CONDENSATION OF PURE FC-72 ($h = 2$ mm AND $p_{in} = 100$ kPa). THE CFD TRANSITION CRITERIA IS IN THE $Re_{in|h} - X$ PLANE AND KIM AND MUDAWAR [12] PREDICTIONS ARE IN $\frac{1}{4} Re_{in}|_{D_h=D} - X$ PLANE.

5.1.1 Theoretical support for quality-based correlations in the form of Eqs. (14-15) and their assessments

Note that, using Eq. (29) to obtain an expression for \hat{x} in terms of $X(\hat{x})$ in the proposed HTC theoretical/computational correlation given in Eq. (23), one obtains a quality based correlation:

$$Nu_x \cong 0.1001(1 - X)^{-0.59} Re_{in}^{0.122} \left(\frac{Ja}{Pr_1}\right)^{0.30} \left(\frac{\rho_2}{\rho_1}\right)^{-0.73} \left(\frac{\mu_2}{\mu_1}\right)^{0.069} \quad (34)$$

for $0 \leq X \leq 1$ with $\frac{Ja}{Pr_1}, \frac{\rho_2}{\rho_1}, \frac{\mu_2}{\mu_1}$ in their ranges given in Table-2.

The dependence on Ja/Pr_1 in Eq. (34) is somewhat weak – because the Ja/Pr_1 term contribution ranges from 0.24 to 0.4 (see Ja/Pr_1 range in Table-2). The dependence on Su , and g_{nd} was already assessed to be weak through direct inspection of the steady solutions ([16-18]). Therefore one may approximately replace Eq. (34) by the form used in the literature and described in Eq. (14). This more approximate form is:

$$Nu_x \approx 0.031(1 - X)^{-0.59} Re_{in}^{0.122} \left(\frac{\rho_2}{\rho_1}\right)^{-0.733} \left(\frac{\mu_2}{\mu_1}\right)^{0.069} \quad (35)$$

Also note that the reduced correlation in Eq. (35), though more approximate than the one in Eq. (34), is of the widely used ([12, 13]) form suggested through Eq. (14). The above argument along with the earlier argument of implied

consistency with the fundamental structure proposed in Eq. (6), establishes the approximate equivalence of the two representations, for HTC correlations.

The results in Eqs. (34-35) are for rectangular channels with aspect ratio $AR \equiv h/w \approx 0$ whereas Kim and Mudawar correlations are for circular and rectangular cross-sections with $AR = D/D_h = w/h \approx 1$. Yet if D was large and the curvature effects could be ignored, the channel correlations $Nu_{x|h}$ and tube-correlations - theoretical ([16-18]) or empirical (Kim and Mudawar [12]) - would satisfy the approximate equalities in Eq. (16). To clearly assess the effects of curvature or AR , a theoretical/computational result is obtained for a shear driven in-tube case with the help of 1-D/2-D CFD approach ([7, 16-18]) whose correlations are reported elsewhere.

To assess the adequacy of the representation in Eq. (34), its result is compared, in Fig. 8 for an FC-72 condensing flow situation, against theoretical/computational results and Kim and Mudawar and others' correlations ([12, 19-21]) applicable for shear driven annular condensing flows. Figure 8 is plotted for a specific case of flow condensation of pure FC-72 in a horizontal channel ($h=2$ mm, $p_{in}=100$ kpa, and $\Delta T=15$ °C) or a tube with $D=4h$. The result in Fig. 8A clearly establishes the consistency of $AR=0$ channel flow computational predictions and the significance of curvature in comparison to in-tube ($AR=1$) computational results. It should be observed that channel results are approximately 90% higher than Kim and Mudawar results ([12]) whereas in-tube results are approximately 30% higher than the Kim and Mudawar empirical results. Since Kim and Mudawar empirical results also cover square and rectangular channel data, and given the $\pm 30\%$ nature of their "curve-fit" with a very large amount of data – the comparisons establish the fidelity of both types of correlations (the computational ones as well as the empirical ones). However our proposals (channel and cylinder) are more reliable on the following counts: (i) our channel flow CFD predictions are in agreement (reported in [16, 17]) with our own experimental results ([3, 4]) for small aspect ratio rectangular cross-sections, and (ii) our flow-physics assumptions of laminar condensate (despite interfacial waves) and laminar vapor flow near interface is consistent with low liquid Reynolds numbers (i.e. $Re_l(x) \equiv Re_\delta = Re_{in} \cdot (\mu_2/\mu_1) \cdot (1-X(x)) < 800$) and vapor-suction at the interface – and these assumptions are superior to the turbulent liquid flow assumptions of Dobson and Chato ([19]) used by Kim and Mudawar to develop their "curve-fit" correlation. Fig. 8B shows the ability to make reliable and consistent "quality X versus distance \hat{x} " predictions with the help of the models in Fig. 8A and the energy equation in Eq. (12) or Eq. (17). Fig. 8C compares our and Kim and Mudawar ([12]) predictions with predictions from correlations of Dobson and Chato ([19]), Wang et al. ([21]), and Shah ([20]). The results in Fig. 8C reinforce the assessment that, for $AR \approx 1$ mm-scale condensers, the Kim and Mudawar curve-fit is more consistent and superior to other empirical curve-fits. Because the in-tube theoretical/computational correlation is close to the more recent correlation of Kim and Mudawar and this work has extensive discussions associated with their correlation in relation to others', it is not necessary for

this paper to focus on merits/demerits of various other correlations (including the ones in Fig. 8C). It should also be noted that the much higher HTC and lower expected pressure drop for channel over in-tube flows suggest that multiple channel condensers with $AR \sim 0$ (as in plate and fin heat exchangers) are superior to multiple millimeter scale rectangular/square channels of $AR \sim 1$.

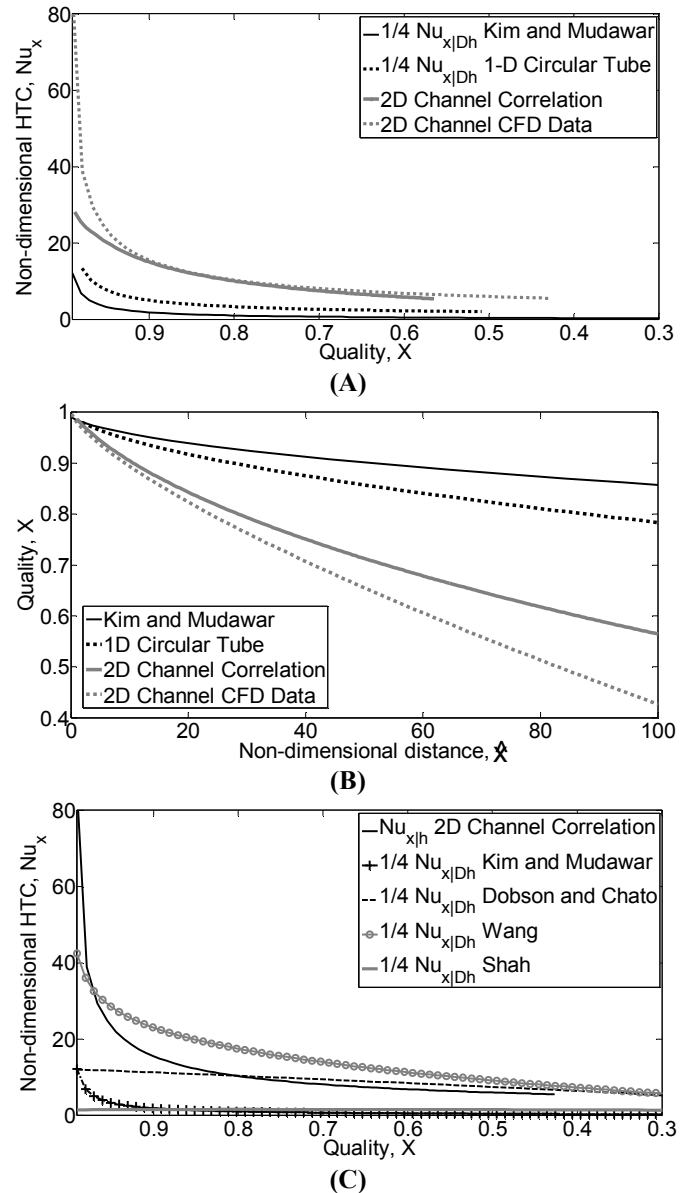


FIGURE 8: THE FIGURE PRESENTS: (A) Nu_x VERSUS QUALITY X CURVES OBTAINED FROM COMPUTATIONS-BASED CORRELATIONS FOR CHANNELS AND $\frac{1}{4} Nu_{x|Dh=D}$ VERSUS X CURVES FOR TUBES [7] AND KIM AND MUDAWAR CORRELATION [12]. (B) THE QUALITY X VERSUS DISTANCE \hat{x} CURVE IS OBTAINED FOR THE MODELS CONSIDERED IN (A). (C) SAMPLE COMPARISONS OF PROPOSED 2-D THEORY BASED CHANNEL CORRELATIONS FOR $Nu_{x|h}$ WITH $\frac{1}{4} Nu_{x|Dh=D}$ VALUES OBTAINED FOR KIM AND MUDAWAR [12], AND OTHERS' CORRELATIONS.

The importance of good correlations for non-dimensional HTC and \hat{x}_A also come from the fact that the next generation of shear driven condensers ([3, 4]) are likely to experience annular condensing flows over the entire length of the device. This is because controlled recirculation of vapor in the innovative devices (see Fig. 9) allow adjustment of vapor flow rates (and thus $X(\hat{x})$ within the device) in a way that the device-length L in Fig. 9 always satisfies $L < x_A$. That is, the controlled rate of vapor recirculation allows one to operate the shear driven condenser in the annular/stratified portions of the flow regime map in Fig.7.

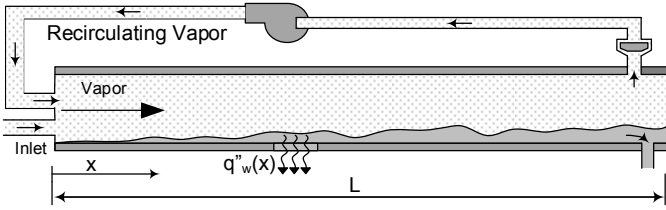


FIGURE 9: THE FIGURE DEPICTS AN INNOVATIVE ALL ANNULAR NON-PULSATILE CONDENSER OPERATION. BOTH PULSATILE AND NON-PULSATILE OPERATIONS ARE DESCRIBED IN [3].

5.1.2 Comments on Possible Uses of Other Non-Dimensional Parameters

Besides the more physics-based non-dimensional parameter set in Eq. (21) and its equivalent “typically followed” empirical correlation structure in Eq. (22), other non-dimensional parameter sets are also possible. Since the non-dimensional governing equations hold for a large class of flows and one is often interested in particular variables (such as Nusselt number Nu_x , etc.) or particular limiting flow classes (thin, thick, or wavy condensate in annular flows), it is conceivable that some other non-dimensional numbers - obtainable from simple power-law combinations of the ones in Eq. (21) – may work and better elucidate the physics underlying a particular situation of interest.

5.2 Relationship between Proposed Popular Quality-Based Maps and Maps in the Physical Parameter Space

As mentioned in section 2, a flow regime map in the $\{Re_{in}, \frac{Ja}{Pr_1}, \hat{x}; \frac{\rho_2}{\rho_1}, \frac{\mu_2}{\mu_1}, Su, g_{nd}\}$ space depicts the transition between the different flow regimes in a much more intuitive fashion than the one in $\{Re_{in}, X, \frac{\rho_2}{\rho_1}, \frac{\mu_2}{\mu_1}, Su, g_{nd}\}$ space marked by transition curves of the type given by Eq. (15). This is because, for a given pure fluid, diameter D_h , and inlet pressure p_{in} ; a condenser sees approximately fixed values of $\{\frac{\rho_2}{\rho_1}, \frac{\mu_2}{\mu_1}, Su, g_{nd}\}$ – whereas the non-dimensional downstream distance (\hat{x}), cooling condition ($\frac{Ja}{Pr_1}$), and inlet mass flow rate (Re_{in}) are the variables that naturally control non-dimensional HTC values (Nu_x) and the length of the annular regime (\hat{x}_A) in experimental observations ([3, 4]) as well as in computational approaches ([16-18]). However, empirical or theoretical flow regime maps (such as the one in the $Re_{in} - X$ space in Fig. 7) can be converted to the

desired map in the three dimensional space of $\{\frac{Ja}{Pr_1}, Re_{in}, \hat{x}\}$ for the representative values of $\rho_2/\rho_1 \cong 0.008, \mu_2/\mu_1 \cong 0.0234, Su \cong 6.44e6$ and $g_{nd} \cong 6.36e6$. For example, to re-map the non-dimensional transition criteria map in Fig. 6 with the help of the Nu_x correlation in Eq. (19), the $X(\hat{x})$ solution of the nonlinear ODE energy equation given in Eq. (12) or Eq. (17) is obtained for a range of Re_{in} and $\frac{Ja}{Pr_1}$ values. The 3-D map for Fig. 6, based on Eq. (16), Eq. (17) and Eq. (19) is shown in Fig. 10. Such maps are helpful in understanding the flow-physics and can always be obtained by the above described procedure and can be presented for our own more reliable ([15-18]) transition criteria in Fig. 7.

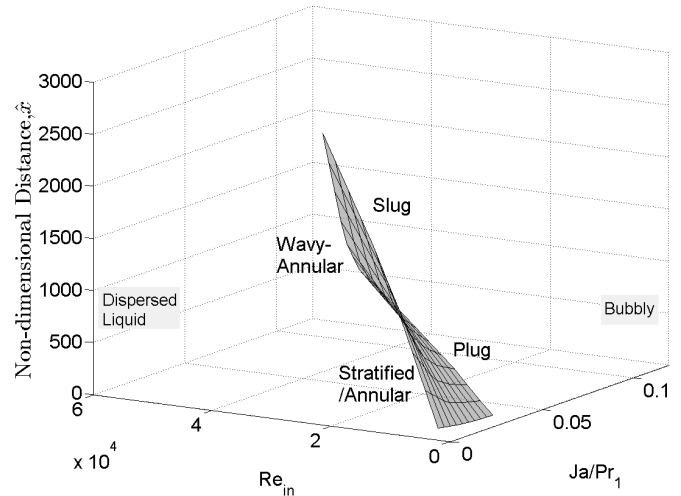


FIGURE 10: THE ABOVE IS A RE-PLOT OF FIG. 6 IN $\{\frac{Ja}{Pr_1}, Re_{in}, \hat{x}\}$ SPACE FOR $\rho_2/\rho_1 \cong 0.008, \mu_2/\mu_1 \cong 0.0234, Su \cong 6.44e6$ AND $g_{nd} \cong 6.36e6$. THE ZONES ARE LABELED AS STRATIFIED ANNULAR, WAVY ANNULAR, PLUG, SLUG, ETC.

5.4 Role of Empirical Correction Factors and its Relationship to Superposed Wave-Structures

It is expected that steady wave-free annular flow CFD solutions and correlations based on them - such as the one in Eq. (23) or in Eq. (35) – may underestimate the HTC value because they ignore wave-effects. Typically 0-20% enhancements are expected ([26]), depending on the amplitude of the superposed wave-structures. Therefore, for specific condenser operations at low to medium Re_{in} , an empirical correction factor “ α ” can be used/developed to adjust the HTC h_x values over its wave-free values through the relation:

$$Nu_x = \alpha [Nu_x |_{Eq.(34)}] \tag{36}$$

For a particular shear-driven condenser operation, α can be adjusted to ensure that the experimental values of heat-flux are closer than the one predicted by Eqs. (34)-(35). Though $1 \leq \alpha \leq 1.2$ is commonly expected, it helps to know the factors that typically govern wave-structures and thus affect the value of α .

5.4.1 Vapor Core Turbulence

The correlations presented here clearly cover parameter space (see Table-2) where $800 \leq Re_{in} \leq 20000$ and vapor core away from the interface is turbulent while the shear driven flow itself is annular/stratified. In most of the shear driven condenser applications, the liquid condensate is thin and liquid film is laminar in the interior – with $Re_\delta < 1000$ [26]. However the interface locations exhibit laminar turbulence in the sense that wave structures have a statistical non-deterministic nature in some of their details. A significant zone of the vapor flow near the interface of the thin condensate is expected to be laminar – this is not only because of the continuity of tangential velocities (which is valid for annular flow boiling and adiabatic two-phase flows as well) but, also, because the normal component of interfacial vapor velocity represents suction of the vapor into the laminar condensate (with significantly reduced normal velocity on the liquid side). Because, for 2D CFD, cell-by-cell velocity determination near the interface is not affected by turbulence in the far field, it correctly simulates the near interface laminar vapor flow. This is the reason why heat-transfer correlations based on laminar-laminar CFD theory work with regard to predicting condensate motion (not far field vapor-core pressure-drops) and heat-transfer rates even for $800 \leq Re_{in} \leq 20000$ (see [16, 17]). The vapor core's turbulence typically affects the amplitude of the wave-structure for non-pulsatile cases but does not significantly affect the length x_A of the annular regime. This fact is discussed in [16, 17] where it is shown that destabilizing energy contents on the laminar film (whether it is within $x < x_A$ or $x \cong x_A$) are rather “sharp” and “peaky” at a particular destabilizing spatial frequency identified as the most dangerous wave-length whereas turbulence related energy content is diffused and spread out over a range of length and time scales.

5.4.2 Role of Exit Conditions

In an actual shear driven condenser or experiments (see [3-5]), a condenser's exit conduction is more likely to be something similar to the arrangement in Fig. 8 rather than the one shown in Fig. 1. The speed with which interfacial waves move forward, i.e. whether they speed up or slow down when they reach the exit, depend on exit conditions (see [16, 17]) and this affects the long time wave-structure and its energy-content present on the mean-interface location. For typical instantaneous film thickness values at wave-troughs (if they are greater than $100 \mu\text{m}$), this wave structure dependence on exit condition is not too large and simple modeling of α , with $1 \leq \alpha \leq 1.2$ in Eq. (36) will suffice.

5.4.3 Pulsatile Flows' Impact on Wave Structures

In the experimental results reported in ([3-5]), if the inlet flow rate in Fig. 8 is made deliberately pulsatile (i.e. there is significant externally imposed amplitude and frequency in the inlet pressure/flow rate), there are large amplitude interfacial waves. This leads to a situation where large amplitude waves are caused by pulsatile vapor dynamics and, concurrently, wave-troughs start “sticking” on a wetting heat-exchange surface (this is observed particularly when the local film-thickness values become less than $0(10\mu\text{m})$). This “sticking” phenomenon leads

to very high heat-fluxes, (see [3]). For such pulsatile cases, α needs to be separately modeled - as $1 \leq \alpha \leq 1.2$ is not typical (instead $3 \leq \alpha \leq 8$ is more common as shown in [3, 5]).

5.5 Pressure-Drop Correlations

For the mm-scale shear driven annular condensation considered here, engineering literature also proposes several pressure-drop correlation (see, e.g. Lockhardt-Martinelli [27]), Friedel [28], etc.). Also there are flow-condensation specific adaptations of pressure-drop correlations in Kim & Mudawar ([12]). Though experiments and theory based synthesis of pressure drop estimates are also possible by an approach similar to the one described here for HTC, such estimates are outside the scope of this paper and are being reported elsewhere (see [15]).

6. CONCLUSIONS

- i. For shear driven annular condensing flows, this paper proposed a first-of-its-kind properly non dimensional heat transfer co-efficient (HTC) correlations. Besides proposing such a correlation based on a fundamental physics-based and theoretical/computational approach, the paper also provides/validates the key foundational ideas for development and assessment of empirical HTC correlations.
- ii. This paper proposed, for the first time, properly non-dimensionalized correlation/map approach for developing/validating criteria for transition from annular to plug/slug flows for shear driven annular condensing flows. Besides assessing existing correlations/maps, it proposes a new criteria which is based on a theoretical/computational instability theory (which is presented elsewhere).
- iii. The importance of coupling quality-based correlation with a one-dimensional energy equation solver - to go back and forth between a reduced indirect parameter space (employing quality) and the physical parameter space in which the flows are observed (involving physical distance) - has been clearly elucidated.
- iv. The proposed correlations are based on steady laminar liquid and laminar vapor CFD solutions for annular/stratified flows. Despite far field (away from the interface) vapor core turbulence, this flow-physics is demonstrated to be effective in estimating heat-transfer rates. Parameters that affect wave-structure and that need development of a well-defined empirical correction factor have been identified.
- v. Because of significant new understanding of flow-physics and CFD tool development (reported elsewhere), the approach presented here provides the foundation for its extension that will also allow development of correlations for pulsatile flows – which are experimentally shown to be promising for development of next generation high heat-flux shear driven condensers.

ACKNOWLEDGMENTS

This work was supported by NSF-CBET-1402702 and NSF-CBET-1033591 grants.

REFERENCES

1. Lasance, C.J.M. and R.E. Simons *Advances In High-Performance Cooling for Electronics*. Electronics Cooling, 2005. **11**.
2. Wilson, J.R. *Electronics Cooling Depends on Innovative Approaches to Thermal Management*. Military & Aerospace Electronics, 2009.
3. Kivisalu, M.T., P. Gorgitrattanagul, and A. Narain, *Results for high heat-flux flow realizations in innovative operations of milli-meter scale condensers and boilers*. International Journal of Heat and Mass Transfer, 2014. **75**(0): p. 381-398.
4. Kivisalu, M.T., et al., *Sensitivity of shear-driven internal condensing flows to pressure fluctuations and its utilization for heat flux enhancements*. International Journal of Heat and Mass Transfer, 2013. **56**(1-2): p. 758-774.
5. Kivisalu, M.T., *Experimental Investigation of Certain Internal Condensing Flows, Their Sensitivity to Pressure Fluctuations and Heat Transfer Enhancements*, in *Mechanical Engineering*. 2015, Michigan Technological University.
6. Carey, V.P., *Liquid-vapor phase-change phenomena : an introduction to the thermophysics of vaporization and condensation processes in heat transfer equipment*. 2nd ed. 2008, New York: Taylor and Francis. xxii, 742 p.
7. Mitra, S., et al., *A quasi one-dimensional method and results for steady annular/stratified shear and gravity driven condensing flows*. International Journal of Heat and Mass Transfer, 2011. **54**(15-16): p. 3761-3776.
8. Taitel, Y. and A.E. Dukler, *A model for predicting flow regime transitions in horizontal and near horizontal gas-liquid flow*. AIChE Journal, 1976. **22**(1): p. 47-55.
9. Baker, O., *Simultaneous flow of Oil and Gas*. Oil and Gas Journal, 1954. **53**: p. 185-215.
10. Coleman, J.W. and S. Garimella, *Two-phase flow regimes in round, square and rectangular tubes during condensation of refrigerant R134a*. International Journal of Refrigeration-Revue Internationale Du Froid, 2003. **26**(1): p. 117-128.
11. El Hajal, J., J.R. Thome, and A. Cavallini, *Condensation in horizontal tubes, part 1: two-phase flow pattern map*. International Journal of Heat and Mass Transfer, 2003. **46**(18): p. 3349-3363.
12. Kim, S.-M. and I. Mudawar, *Review of databases and predictive methods for heat transfer in condensing and boiling mini/micro-channel flows*. International Journal of Heat and Mass Transfer, 2014. **77**(0): p. 627-652.
13. Kim, S.-M. and I. Mudawar, *Universal approach to predicting two-phase frictional pressure drop for adiabatic and condensing mini/micro-channel flows*. International Journal of Heat and Mass Transfer, 2012. **55**(11-12): p. 3246-3261.
14. Tibirić, C.B., G. Ribatski, and J.R. Thome, *Saturated flow boiling heat transfer and critical heat flux in small horizontal flattened tubes*. International Journal of Heat and Mass Transfer, 2012. **55**(25-26): p. 7873-7883.
15. Ravikumar, S., *Fundamental Assesments and New Enabling Proposals for Heat Transfer Correlations and Flow Regime Maps for Shear Driven Condensers in the Annular/Stratified Regime*, in *Mechanical Engineering*. 2015, Michigan Technolgoical University: Houghton, Michigan USA.
16. Naik, R., *Development of unsteady two-dimensional computational simulation tools that simulate annular internal condensing flows and characterize interfacial waves, flow stability and flow sensitivity*, in *Mechanical Engineering - Engineering Mechanics 2015*, Michigan Technological University: Houghton, MI.
17. Naik, R., S. Mitra, and A. Narain, *Steady and Unsteady Simulations that Elucidate Flow Physics and Instability Mechanisms for Annular/Stratified Internal Condensing Flows inside a Channel*. Being Submitted for publication in Journal of Computational Physics, 2015.
18. Naik, R., S. Mitra, and A. Narain, *Steady and Unsteady Computational Simulations for Annular Internal Condensing Flows in a Channel*, in *Proceedings of 2014 ASME International Mechanical Engineering Congress and Exposition*. 2014: Montreal, Canada.
19. Dobson, M.K. and J.C. Chato, *Condensation in smooth horizontal tubes*. Journal of Heat Transfer-Transactions of the Asme, 1998. **120**(1): p. 193-213.
20. Shah, M.M., *A General Correlation for Heat Transfer during Film Condensation inside Pipes*. International Journal of Heat and Mass Transfer, 1979. **22**: p. 547-556.
21. Wang, W.W., *Condensation and single-phase heat transfer coefficient and flow regime visualization in micro-channel tubes for HFC-134a*. 1999, Ohio State University: Ohio.
22. Narain, A., et al., *Direct computational simulations for internal condensing flows and results on attainability/stability of steady solutions, their intrinsic waviness, and their noise sensitivity*. Journal of Applied Mechanics, 2004. **71**(1): p. 69-88.
23. Liang, Q., X. Wang, and A. Narain, *Effects of gravity, shear and surface tension in internal condensing flows: Results from direct computational simulations*. Journal of Heat Transfer, 2004. **126**(5): p. 676-686.
24. Okiishi, T.H., et al., *Fundamentals of fluid mechanics*. 2013, Hoboken, NJ: John Wiley & Sons, Inc.
25. MATLAB Documentation, Mathworks.
26. Bergman, T.L., et al., *Fundamentals of heat and mass transfer*. 7th ed. 2011, Hoboken, NJ: Wiley. xxiii, 1048 p.
27. Lockhart, R.W. and R.C. Martinelli, *Proposed correlation of data for isothermal two-phase, two-component flow in pipes*. Chemical Engineering Progress, 1949. **45**: p. 39-48.
28. Friedel, L. *Improved friction pressure drop correlations for horizontal and vertical two-phase pipe flow*. in *European Two-phase Group Meeting*. 1979. Ispra, Italy.